Mode-distribution analysis of quasielastic neutron scattering and application to liquid water

Tatsuya Kikuchi,[1] Kenji Nakajima,[1] Seiko Ohira-Kawamura,[1] Yasuhiro Inamura,[1] Osamu Yamamuro,[2] Maiko Kofu,[2] Yukinobu Kawakita,[1] Kentaro Suzuya,[1] Mitsutaka Nakamura,[1] and Masatoshi Arai[1]

[1]*Neutron Science Section, J-PARC Center, Tokai, Ibaraki 319-1195, Japan*

[2]*ISSP-NSL, University of Tokyo, Tokai, Ibaraki 319-1106, Japan*

(Received 15 October 2012; revised manuscript received 25 February 2013; published 19 June 2013)

A quasielastic neutron scattering (QENS) experiment is a particular technique that endeavors to define a relationship between time and space for the diffusion dynamics of atoms and molecules. However, in most cases, analyses of QENS data are model dependent, which may distort attempts to elucidate the actual diffusion dynamics. We have developed a method for processing QENS data without a specific model, wherein all modes can be described as combinations of the relaxations based on the exponential law. By this method, we can obtain a distribution function $B(Q,\Gamma)$, which we call the mode-distribution function (MDF), to represent the number of relaxation modes and distributions of the relaxation times in the modes. The deduction of MDF is based on the maximum entropy method and is very versatile in QENS data analysis. To verify this method, reproducibility was checked against several analytical models, such as that with a mode of distributed relaxation time, that with two modes closely located, and that represented by the Kohlrausch-Williams-Watts function. We report the first application to experimental data of liquid water. In addition to the two known modes, the existence of a relaxation mode of water molecules with an intermediate time scale has been discovered. We propose that the fast mode might be assigned to an intermolecular motion and the intermediate motion might be assigned to a rotational motion of the water molecules instead of to the fast mode.

DOI: 10.1103/PhysRevE.87.062314 PACS number(s): 66.10.C−, 78.70.Nx

I. INTRODUCTION

Several experimental techniques have been proposed for studying molecular and atomic dynamics. Among them, quasielastic neutron scattering (QENS) obtains a dynamic structure factor $S(Q,\omega)$ that provides space and time information on diffusion dynamics [1]. QENS data are essentially only one peak of intensity variation against energy transfer. All information about interesting properties of the system with regard to relaxation, local motion, and diffusion is included in the shape of this peak. Conventionally, fittings based on various diffusion models have been conducted to obtain physical quantities [1].

In general, the simple relaxation mode is described by exponential decay with single characteristic decay time, that is, relaxation time. This assumption is based on diffusion according to Fick's law or relaxation occurring by a stochastic process such as a transition process between double wells. Diffusion models used in conventional analysis are usually supported from other experimental results. In most cases, such a model is composed of one or two modes, although it is known that diffusion processes in materials are quite complicated. In addition, how appropriately the number of modes is chosen always remains an open discussion.

We propose an analysis using the maximum entropy method (MEM) [2,3] to resolve this uncertainty in the analysis. By this method, the number of modes and the distribution of the relaxation time in the modes can be obtained. In this method, we first supposed that all modes can be described as combinations of the relaxations based on the exponential law, and the intermediate scattering function $F(Q,t)$ is written as

$$F(Q,t) = A(Q) + \int B(Q,\tau)\exp\left(-\frac{t}{\tau}\right)d\tau, \qquad (1)$$

where $A(Q)$ is the elastic intensity of a neutron scattering. $B(Q,\tau)$ is a new distribution function to show the number of modes and distributions of the relaxation times in the modes and we call it the mode-distribution function (MDF). Executing Fourier transformation on t, the dynamic structure factor $S(Q,\omega)$ can be written by use of the Lorentz function as

$$S(Q,\omega) = A(Q)\delta(\omega) + \int B(Q,\Gamma)\frac{1}{\pi}\left(\frac{\Gamma}{\omega^2+\Gamma^2}\right)d\Gamma, \qquad (2)$$

where Γ is the width of the Lorentz function and $B(Q,\Gamma)$ is a variable-transformed MDF function obtained from $B(Q,\tau)$.

Such analysis to elucidate the distribution of relaxation time to study the dynamics is widely done by using the dynamic light scattering (DLS) combined with the CONTIN program [4]. Since measurement time ranges of QENS are narrower than DLS in general, reliability of the results from QENS can be less than those from DLS in the time space. Still however, in the case of QENS, obtained distribution also has information in momentum space (Q). Therefore, even with narrower time range, reliable and rich information can be obtained by measuring the change of Q. Also, one should note that integrated intensity of QENS spectrum is equivalent to integrated intensity of the distribution of the relaxation time, which causes much advantage in mathematical operation.

An example of this function of the constant Q is shown in Fig. 1. $B(Q,\Gamma)$ consists of a few peaks in most cases. Each peak represents several characteristics of single relaxation. The peak position corresponds to the average relaxation time, and the peak area reflects the number of atoms or the ratio of moving atoms to the total atoms. In addition, our analysis method provides new information about the nonuniformity of the dynamics. The peak width and shape represent the distribution of relaxation time caused by differences in the local structure. The Q dependencies of the peaks represent the spatial feature of motions. Because this function can not be calculated by conventional analyses, the number of modes has been limited and the distribution of the relaxation times

 ©2013 American Physical Society

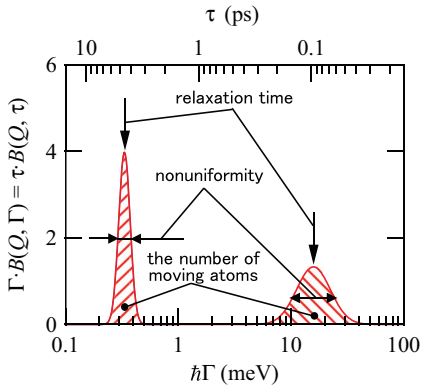

FIG. 1. (Color online) Example of a mode-distribution function (MDF) on constant Q.

has not been considered to date in many cases. By using our analysis method, we can directly calculate this MDF from QENS measurement data.

However, there is an inverse problem in the calculation of MDF. Both statistical errors and experimental errors can greatly affect the result when a simple least squares method is used because the energy range of a measurement is limited, whereas the Lorentz function has wing tails over a wide energy range. We adopted MEM in our analysis method to avoid this problem and appropriately deal with the errors on the basis of information theory.

In Sec. II, we expound on the details of our analysis method. The validity of this method is examined by several groups of simulated data in Sec. III. We report the first application of our analysis method to real matter, chosen to be liquid water, in Sec. IV. Liquid water is a material that has interested many researchers for a long time, but controversy surrounds the various diffusion models that have been proposed. Therefore, liquid water is a suitable but challenging material to demonstrate the capability of our model-free analysis method.

II. ANALYSIS METHOD

The essential part of this study is the deduction of $B(Q,\Gamma)$ from $S(Q,\omega)$ by Eq. (2). In our procedure, we discretized $B(Q,\Gamma)$ into equally spaced discrete Γ in logarithmic space. We convoluted the resolution function $\Re(Q,\omega)$ and added background to Eq. (2). Then, the dynamic structure factor $S_{\rm cal}(Q,\omega)$ was written as follows:

$$S_{\rm cal}(Q,\omega) = A(Q)\Re(Q,\omega) + \sum_i^N B(Q,\Gamma_i)\left[\Re(Q,\omega)\otimes\frac{1}{\pi}\left(\frac{\Gamma_i}{\omega^2+{\Gamma_i}^2}\right)\right] + \text{background}. \quad (3)$$

The second term on the right side is multiplied by the coefficient Γ_i, which is derived from discretization in logarithmic space. $B(Q,\Gamma_i)$ can be calculated at individual Q.

The obtained $B(Q,\Gamma_i)$ is the simplest distribution involving the least information, that is, maximizing information entropy, among all distributions that sufficiently reproduce the given experimental data within statistical errors. Distortion of the solution by statistics errors, experimental errors, and limitations of measurable range can be minimized in this method. MEM is a general inference method based on the theory of information entropy and provides a way to approach the inverse problem. It is often applied in the fields of image processing and signal processing. In addition, the MEM-Rietveld method [5,6] has been performed for the past two decades to deduce electron density distribution in x-ray scatterings and nuclear density distribution in neutron scatterings.

In our MEM method, we introduce information entropy S for the mode-distribution function as a measure of simpleness:

$$S = -\sum_i^N \left[X_i \ln\frac{X_i}{m_i} + m_i - X_i\right], \quad (4)$$

where

$$X_i = \Gamma_i \sum_i^N B(Q,\Gamma_i), \quad (5)$$

and m_i is defined as the simplest distribution without any information from experimental data. The entropy becomes maximum at $\{X_i\} = \{m_i\}$. We set m_i to a constant value as the highest entropy state for the information theory. The reproducibility of the experimental data is measured by the χ^2 statistic as follows:

$$F = \chi^2/2 - \alpha S, \quad (6)$$

where α is an undetermined positive coefficient that controls how closely the solution fits the data. The solution is X_i to minimize this quality factor at a specific α. The optimal $\alpha = \hat{\alpha}$ is determined by

$$-2\alpha S = \sum_i^N \frac{\lambda_i}{\hat{\alpha}+\lambda_i}, \quad (7)$$

where λ_i is an eigenvalue of the Hessian operator $\partial^2\chi^2/\partial X_i\partial_j$. This determination procedure in the MEM solution is called classic MEM. The actual calculations were performed with our in-house code that was composed for the present analyses.

III. GENERAL PROPERTIES OF MODE-DISTRIBUTION ANALYSIS

To examine the validity of our analysis method, we applied it to several types of modeled spectra assuming typical relaxation modes. The mock spectra $S(Q,\omega)$ were obtained in the range -6 to 6 meV as a constant Q function and were convoluted by a Gaussian-type resolution function with a full width at half maximum of 0.1 meV. Under these conditions, QENS data obtained with a neutron incident energy of about 7 meV and a ratio of energy resolution to incident energy of about 1.5% can be simulated. To be a realistic model, the statistical error of neutron scattering described by the Poisson distribution was added to the spectrum, supposing that 105 neutrons were counted in the entire range of the spectrum.

A. Case I: Single relaxation

First, we demonstrated the method by applying it to the single relaxation derived from elemental motion as a typical

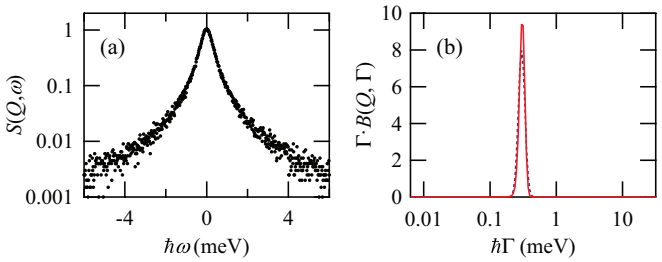

FIG. 2. (Color online) (a) Dynamic structure factor $S(Q,\omega)$ and (b) mode-distribution function $B(Q,\Gamma)$ of a single relaxation mode with narrower Gaussian-distributed relaxation time calculated using Eq. (8) ($\hbar\Gamma_0 = 0.3$ meV, $\sigma = 0.05$). In (b), the original spectrum and the analysis results are shown by dotted and solid lines, respectively.

relaxation model, where the relaxation time has Gaussian distribution in logarithmic space. Under this supposition, $B(Q,\Gamma)$ multiplied by Γ is expressed as

$$\Gamma B(Q,\Gamma) = \frac{1}{\sqrt{2\pi}\sigma} \exp\left[\frac{(\ln\Gamma - \ln\Gamma_0)^2}{2\sigma^2}\right], \qquad (8)$$

where Γ_0 is the peak position and σ is the standard deviation. Figure 2(a) shows $S(Q,\omega)$, which was calculated by this equation with $\hbar\Gamma_0 = 0.3$ meV and $\sigma = 0.05$. Figure 2(b) shows the result obtained from the mode-distribution analysis. In addition, the case of a wider mode distribution $S(Q,\omega)$, with $\hbar\Gamma_0 = 0.3$ meV and $\sigma = 0.2$, was also demonstrated, as shown in Fig. 3. Although, at a glance, we can not see clear differences in $S(Q,\omega)$ between the narrower [Fig. 2(a)] and wider [Fig. 3(a)] mode distributions, this method can distinguish original widths, as seen in Figs. 2(b) and 3(b).

B. Case II: Slow and fast limitations

To examine the computable Γ range, we assume slow and fast limit relaxations; the width of the slow limit relaxation is narrower than the resolution's width, and the width of the fast limit relaxation is about the maximum energy of the spectrum. $B(Q,\Gamma)$ for slow and fast relaxations is represented in Eq. (8) with $\hbar\Gamma_0 = 0.02$ meV, $\sigma = 0.1$ and with $\hbar\Gamma_0 = 3$ meV, $\sigma = 0.1$, respectively. $S(Q,\omega)$ in this model and the result of the analysis are shown in Fig. 4. The figure shows that the analysis is quite possible in the range of this level, although the reproducibility is lower than the result seen in Fig. 2.

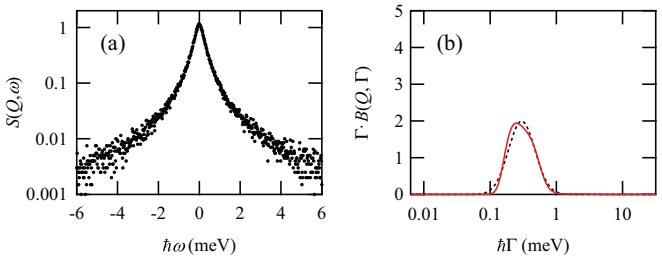

FIG. 3. (Color online) (a) Dynamic structure factor $S(Q,\omega)$ and (b) mode-distribution function $B(Q,\Gamma)$ of a single relaxation mode with wider Gaussian-distributed relaxation time calculated using Eq. (8) ($\hbar\Gamma_0 = 0.3$ meV, $\sigma = 0.2$). In (b), the original spectrum and the analysis results are shown by dotted and solid lines, respectively.

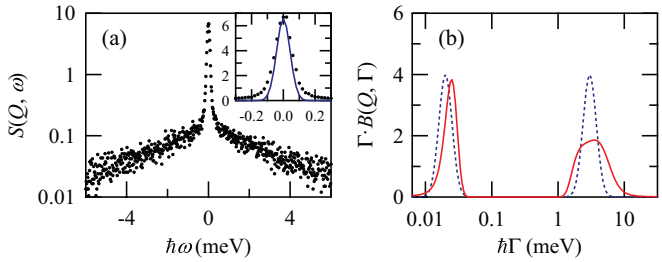

FIG. 4. (Color online) (a) Dynamic structure factor $S(Q,\omega)$ and (b) mode-distribution function $B(Q,\Gamma)$ of a model with slow and fast limit motions represented by Eq. (8) ($\hbar\Gamma_0 = 0.02$ meV, $\sigma = 0.1$ and $\hbar\Gamma_0 = 3$ meV, $\sigma = 0.1$, respectively). The solid line in inset of (a) shows the resolution. In (b), the original spectrum and the analysis results are shown by dotted and solid lines, respectively.

The reproducible Γ range must be from the slowest time limit in the relaxation process at the resolution width to the fastest limit at the maximum energy of the spectrum. In fact, Fig. 4 shows that the analysis is quite possible in such a range, although the reproducibility is fair, where $B(Q,\Gamma)$ for the slow relaxation of $\hbar\Gamma_0 = 0.02$ meV, $\sigma = 0.1$ and the fast relaxation of $\hbar\Gamma_0 = 3$ meV, $\sigma = 0.1$ is verified.

C. Case III: Separation of modes

We mentioned that the number of modes in the dynamics is obtained by our analysis method. There must be difficulties in separating the two modes when they have similar relaxation times. Figure 5 shows an example of two closely located relaxation modes calculated by Eq. (8) with $\hbar\Gamma_0 = 0.1$ and 0.4 meV, where the modes could be separated surely. We confirmed that the capability to separate two closely located modes obviously depends on the statistics precision and the energy range of the experimental data.

D. Case IV: Diffusion by the KWW function

In conventional QENS analysis, the Kohlrausch-Williams-Watts (KWW) function is often utilized. In the space of the intermediate scattering function, the KWW function represents

$$F(Q,t) = \exp\left[-\left(\frac{t}{\tau}\right)^{\beta}\right], \qquad (9)$$

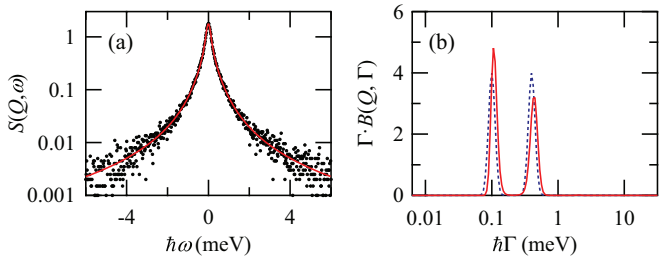

FIG. 5. (Color online) (a) Dynamic structure factor $S(Q,\omega)$ and (b) mode-distribution function $B(Q,\Gamma)$ of a model with two closed relaxation time modes represented by Eq. (8) ($\hbar\Gamma_0 = 0.1$ meV, $\sigma = 0.05$ and $\hbar\Gamma_0 = 0.4$ meV, $\sigma = 0.05$). Solid line shows the fit to $S(Q,\omega)$. In (b), the original spectrum and the analysis results are shown by dotted and solid lines, respectively.

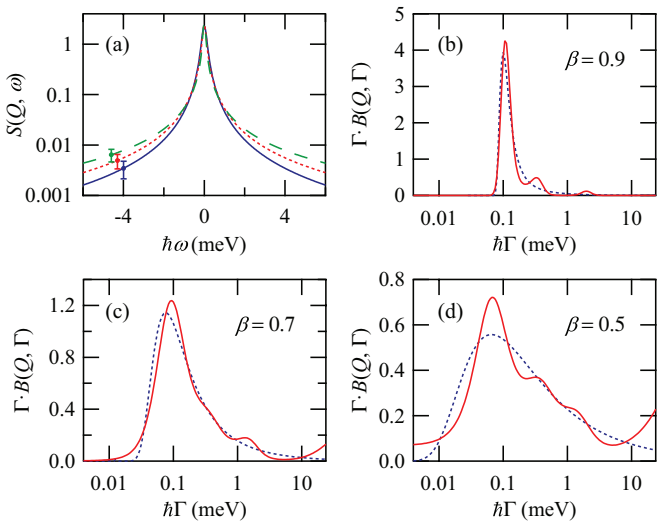

FIG. 6. (Color online) (a) Dynamic structure factor $S(Q,\omega)$ of models by the KWW function with $\tau = 5$ ps and $\beta = 0.9$ (solid line), 0.7 (dotted line), and 0.5 (dashed line). (b)–(d) Mode-distribution function $B(Q,\Gamma)$s of these models; (b) $\beta = 0.9$, (c) $\beta = 0.7$, and (d) $\beta = 0.5$. In (b)–(d), the original spectrum and the analysis results are shown by dotted and solid lines, respectively.

where β is an index of the stretched exponential. The Fourier transform of this function is needed to calculate $S(Q,\omega)$. It can be performed only by numerical integration because the analytical results of the Fourier transform of this function are not derived. In addition, the KWW function can be described as an integral of exponential decay relaxations [7,8] or $B(Q,\Gamma)$ of this model can be directly transformed. Figure 6 shows $S(Q,\omega)$s and $B(Q,\Gamma)$s with $\tau = 5$ ps and $\beta = 0.9$, 0.7, and 0.5. As seen in this figure, $B(Q,\Gamma)$s of the KWW function are asymmetric distributions with long tails on the right side, and the distributions become wider with increasing β. We applied the mode-distribution analysis to calculate $S(Q,\omega)$'s by the KWW function. The results of the analysis are shown in Figs. 6(b)–6(d). The $B(Q,\Gamma)$s of the analysis results consist of about three peaks broadened widely, but roughly conforming to the transformed distributions. Because the information entropy of the asymmetrically distributed relaxation represented by the KWW function is low in our analysis method, the reproducibility of the shapes is not so good. The origin of the inability to reproduce $B(Q,\Gamma)$ derived from the KWW function may relate to a large difference in the basic principle between our method and the relaxation by the KWW function. Because our method is based on simple exponential decay as a unit relaxation, motions represented by the KWW function have low information entropy; that is, a more informative state is difficult to reproduce properly in our method.

IV. APPLICATION TO LIQUID WATER

A. Background

For the first application of the analysis method, we chose liquid water as a typical sample for a QENS experiment. Although water is a relatively simple material consisting of H_2O molecules, its diffusion is rather complicated. In particular, the local motions of water molecules still have not been determined clearly. As for QENS, since the earliest studies in the 1970s [9], many experiments have been conducted on water and related materials to date, subsequently producing various diffusion models of liquid water (e.g., the traditional multiple exponential time-decay model [10,11], the translation-rotation coupling of molecular motion [12,13], and the relaxing-cage scheme [14]). The studies on this subject have been conducted recently [15].

B. Experimental details

The QENS experiment on liquid water at ambient temperature was conducted on AMATERAS, a cold-neutron disk chopper spectrometer, installed at the spallation neutron source of the Materials and Life Science Experimental Facility (MLF) at J-PARC [16]. The sample was loaded into an aluminum double-cylinder cell (wall of diameter 14 mm and thickness 0.3 mm). The weight of the sample was 0.6 g.

AMATERAS can perform multiple incident energy (multi-E_i) measurements by repetition rate multiplication [17,18]. Therefore, one can simultaneously perform high-resolution measurements with low E_i's and wide energy-range measurements with high E_i's. Our analysis method is quite suitable for such a measurement with wide time-scale relaxations. The selected E_i's in the present experiments are 1.68, 3.13, and 7.74 meV. The resolutions of those E_i's were 17, 35, and 121 μeV, respectively. Under these conditions, time ranges from 0.1 to 100 ps are accessible. Data acquisition time was 4 h with J-PARC operation at a 120-kW proton-beam power. We also measured a vanadium cylinder, 14 mm in diameter and 0.3 mm thick, as a standard sample for estimating constant background and intensity corrections and for obtaining the resolution function, which are required in our fittings.

C. Results

The data obtained after a series of corrections, such as a background correction and an intensity correction among different E_i's, are shown in Fig. 7. Multiple scattering in the data has also been corrected on the basis of a simulated multiple scattering spectrum. The QENS spectrum for light liquid water is mainly contributed by the self-diffusion of hydrogen atoms because the light hydrogen atom has quite a large incoherent scattering cross section (19 times larger than the total scattering cross section of the oxygen atom). For $E_i = 1.68$, 3.13, and 7.74 meV, covered Q ranges of the data are 0.2–1.3 Å^{-1}, 0.2–1.9 Å^{-1}, and 0.3–3.0 Å^{-1}, respectively. For each Q, we used as much as possible data. Especially, in the range of $0.3 < Q < 1.9$ Å^{-1}, three spectra obtained by three different E_i's were fitted simultaneously to improve the precision and reliability of the results in our analysis. The typical spectra at $Q = 1.0$ Å^{-1} after the series of corrections are shown in Fig. 8 with a fitted function. The obtained $B(Q,\Gamma)$ has three components as seen in Fig. 9. Each component may correspond to water molecules with different diffusional motions of water molecules. Hereafter, we call them slow, intermediate, and fast components in the relaxation time axis on the left. Each contribution to $S(Q,\omega)$ is also shown in Fig. 8 by dotted, dashed, and dashed-dotted lines, respectively.

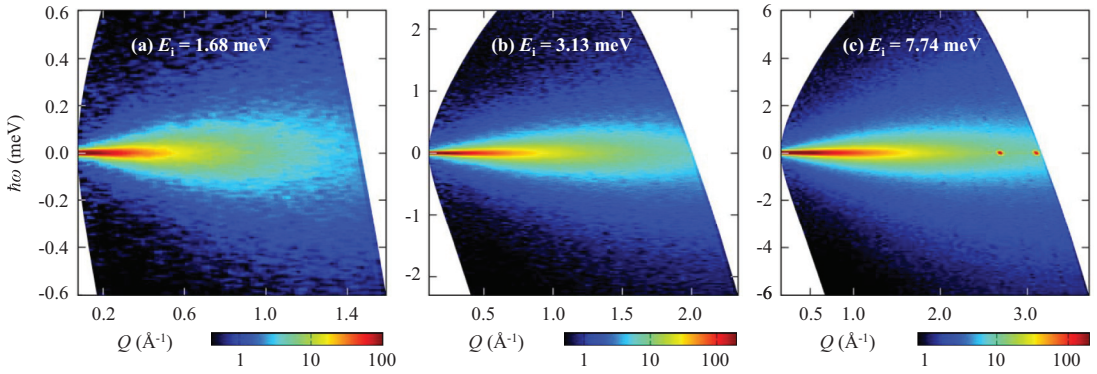

FIG. 7. (Color) QENS spectra for H_2O liquid at ambient temperature. Three E_i's were used in one measurement: (a) 1.68 meV, (b) 3.13 meV, and (c) 7.74 meV. Colors represent the intensity of the QENS spectra. Sharp peaks at $Q = 2.7$ and 2.1 Å^{-1} at elastic position are Bragg reflections from Al and subtracted in the fitting process.

A full picture of $B(Q,\Gamma)$ is shown in Fig. 10. The Q dependencies of the three components are clearly seen. These peaks are substantially sharp, which indicates that relaxations of these components are almost homogeneous. In other words, each relaxation is an approximately simple relaxation. We can characterize these peaks by their intensities (as shown in Fig. 11) and peak positions.

The intensity of the slow component is relatively large in all ranges of Q and decreases with increasing Q in a high-Q region. The peak position of this component is strongly shifted from small Γ to large Γ as Q increases in the middle-Q region and is almost constant in the higher-Q region. Relatively higher intensity in all Q regions and large Q dependence of the peak position in the low-Q region indicate that the slow component is related to a translational diffusion. Small Q dependence of the peak position in the higher-Q region can be accounted for by considering the motion as a series of jumps and not a continuous translation.

On the other hand, the intensity of the fast component increases with Q. This component can not be seen in a low-Q region. The peak maintains almost the same Γ position. The disappearance of intensity in a low-Q region indicates that the fast component is a motion in a limited space. This motion corresponds to a water molecule motion previously considered to be rotational motion in early studies by the INS [11].

These two components have been reported in earlier investigations on the diffusion of liquid water [11–13]. In the current investigation, we found a third component, that is, an intermediate component, which has not been reported so far. The intensity of the intermediate component is weak and is merged into the slow component in the range $Q > 1.2$ Å^{-1}. The peak position shows weak Q dependence. We will discuss these three components in the next section.

D. Analysis and discussion of each component

1. Slow component

Translational diffusion of this component is considered to be a series of jumps. The classical jump diffusion model is suitable for this component. This model has also been used in the analysis of the translational motion of water molecules in earlier studies [11–13]. The model approximately represents a motion of repeating jumps between distant places after some residence time. Given a mean jump length L and a mean residence time τ_0, the diffusion coefficient D and Γ can be described as

$$D = \frac{L^2}{6\tau_0}, \tag{10}$$

$$\Gamma = \frac{DQ^2}{1 + DQ^2\tau_0}. \tag{11}$$

We analyze Q dependence of the peak position of the slow component by fitting to this equation. Because the slow component can not be separated from the intermediate component

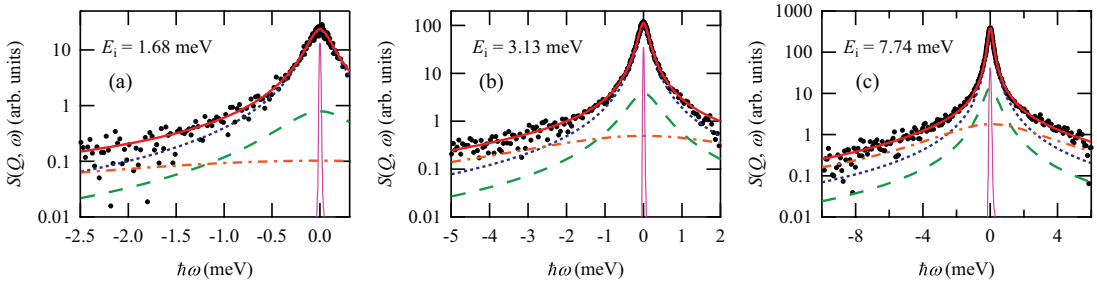

FIG. 8. (Color online) Measured spectra by multi-Ei and fitting results for H_2O at RT and $Q = 1.0$ Å^{-1}. Symbols are experimental data. (a), (b), and (c) are spectra with $E_i = 1.68$, 3.14, and 7.74 meV, respectively. Thick solid lines are $S(Q,\omega)$ obtained by fitting with Eq. (3). Other lines represent the contributions of slow components (dotted lines), intermediate components (dashed lines), and fast components (dashed-dotted line). Thin solid lines are the resolution functions obtained by measuring the vanadium cylinder sample.

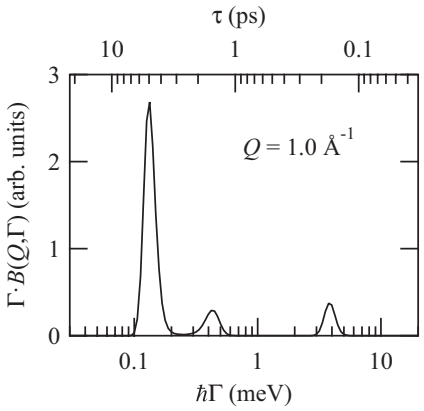

FIG. 9. Intensity distribution of the Lorentz function $B(Q,\Gamma)$ from H_2O at RT and $Q = 1.0$ Å^{-1} obtained in the present analysis.

in the high-Q range, we analyzed the slow component in the range $Q > 1.2$ Å^{-1}. In the results, we obtained a good fitting, as shown in Fig. 12. The obtained parameters are $D = (2.27 \pm 0.05) \times 10^{-5}$ cm^2 s^{-1}, $\tau_0 = 0.46 \pm 0.10$ ps, and $L = 0.79 \pm 0.09$ Å and are comparable with those obtained in the earlier studies [11,15]. Therefore, the motion of this component must be the same as the translational motion in the conventional analyses.

2. *Fast component*

As we mentioned above, the fast component is due to a motion in a limited space. Assuming that Γ is strictly constant, the necessary and sufficient condition of the diffusion model can be derived; that is, a model in which several sites (a few sites or many sites) movable for the atom are relatively fixed and the moving ratio per time between sites is dependent only on the destination site and is independent of the departure site. We propose two models that are derived by this condition.

The first is a model of a few fixed sites. In this model, a few sites are available to the moving atom with the same distance.

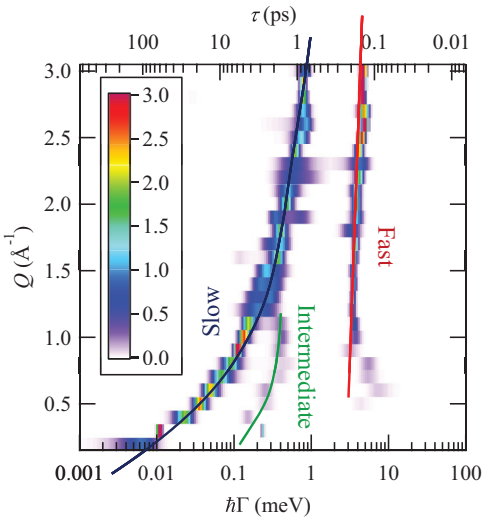

FIG. 10. (Color) Map of the intensity distribution of the Lorentz function $B(Q,\Gamma)$ from H_2O at RT. Colors represent the intensity of $\Gamma B(Q,\Gamma)$.

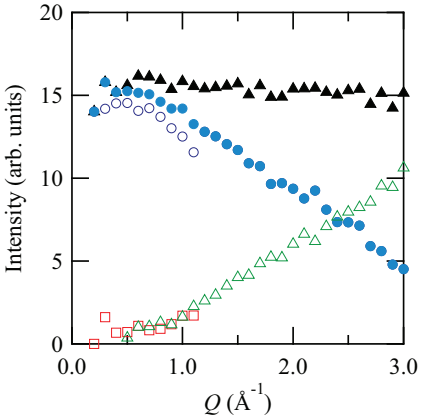

FIG. 11. (Color online) Intensities of individual components and summations of some components; slow component (open circle), intermediate component (open square), fast component (open triangle), sum of slow and intermediate components (filled circle), and sum of all components (filled triangle). In the Q range larger than 1.1 Å^{-1}, the slow and intermediate components become one component. In this range, its intensity is regarded as the sum of intensities of the two components.

The particle, atom or molecule, jumps to the site after staying at the other site for a certain interval. Residence time and jump probability are also assumed to be constant in each site so that relaxation times are the same for all destinations. In this first model, Γ can be written as follows:

$$\Gamma = \frac{2\pi N_{\text{site}}}{t_1}, \tag{12}$$

where N_{site} is the number of the site available to the jumping atom and t_1 is the residence time. As shown in this equation, Γ is independent of Q. The elastic incoherent structure factor (EISF) can be written as

$$I_{\text{EISF}}(Q) = \frac{1}{N_{\text{site}}} + \left(1 - \frac{1}{N_{\text{site}}}\right) j_0(Qd), \tag{13}$$

where d is the distance between the sites and j_0 is the spherical Bessel function of the first kind order 0. In our analysis,

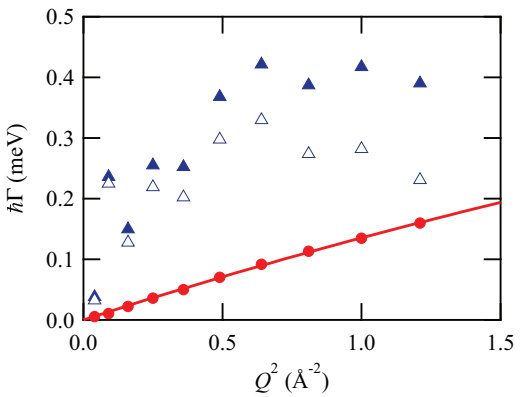

FIG. 12. (Color online) Average peak positions of slow (filled circle) and intermediate components (filled triangle). The open triangle represents the difference between the intermediate component and the slow component. The line is obtained by fitting the slow component with the jump diffusion model, Eqs. (10) and (11).

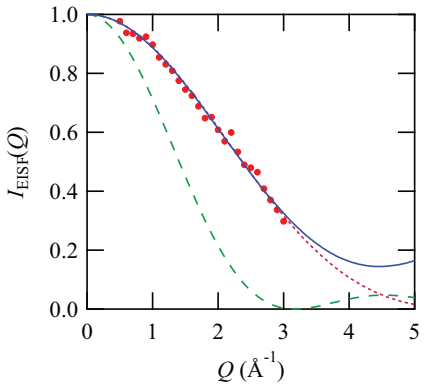

FIG. 13. (Color online) Q dependency of EISF, obtained from the intensity ratio of the slow and intermediate components to the total. The solid line is a fit by the fixed sites model [Eq. (13)], the dotted line is a fit by the free jump region model [Eq. (14)], and the dashed line is the EISF for a spherical surface of radius 0.98 Å, as in the Sears expansion [10].

EISF was regarded as the ratio of the sum of the intensities between the slow and intermediate components to the total intensity. In general, EISF represents the intensity ratio of the elastic component to the total one. In the case the system contains several motions as the present one, and when we focus on the faster motion, we consider that the remaining slower motions can be regarded as elastic component. By fitting experimental data to Eq. (13) as shown in Fig. 13, N_{site} and d were determined to be 3.37 ± 0.47 and 1.007 ± 0.043 Å, respectively. The obtained N_{site} is reasonable for the dimension of space and d is of the same order as the intermolecular distance, considering the O-H distance of 0.99 Å in the literature [19]. Therefore, this model is appropriate rather than the standard rotational model by the Sears expansion [10]. From this result, the motion in this first model must be a rotational motion that switches hydrogen bondings.

We propose another model to satisfy the condition of the Γ constant, which is assumed to be an intermolecular motion whereas the motion in the first model is a rotation of a molecule. In this second model, atoms in a specific region can jump freely within the same region. The number of sites is meaningless. The destination site of the jump does not depend on the departure site, and residence time and jump probability are also constant and independent from the departure and destination sites. When the free jump region is a single sphere with a radius of R, the EISF can be written as

$$I_{EISF}(Q) = \frac{9\,[\sin(QR) - QR\cos(QR)]^2}{(QR)^6}. \qquad (14)$$

By fitting to Eq. (14), R was determined to be 0.766 ± 0.005 Å, as shown in Fig. 13. This free jump region is similar to the basin in the study of MD simulation [15]. We also consider the model of the diffusion inside a sphere with impermeable boundaries. In this model, EISF also follows Eq. (14), although Γ deviates from a constant value in the high-Q range. In order to clearly determine between the two models, a measurement in higher-Q range. In both models, the radius of the confined space is shorter than O-H distance of water molecules and the motion is highly localized. We thought that this motion is like a fluctuation without breaking the local correlation structure. We thought that this second model approximates the actual motion of the fast component better than the first model. In our future studies, higher-Q data must allow us to validate the two models.

3. *Intermediate component*

We consider two possibilities as a motion of the intermediate component. The first is a translational motion of a water molecule in different local surroundings from the case of the slow component. The relaxation time of the motion is simply calculated as the inverse of Γ. Γ of the peak position of the intermediate component is shown in Fig. 12. The Q dependence of Γ resembles that of translational motion, such as the slow component. But, the intensity of the intermediate component decreases with decreasing Q in contrast to the slow component, as seen in Figs. 10 and 11.

The second possibility is an additional motion of the atom during the motion of the slow component. In this case, the relaxation time of the motion is calculated as the inverse of the difference in Γ between the intermediate and slow components. The difference in Γ at the peak position between the intermediate and slow components is shown in Fig. 12. Since the atom already participates in the translational diffusion, which is described as the slow component, it is unlikely that the intermediate component is attributed to a long-distance diffusion motion. Therefore, Γ is possibly almost constant in the low-Q range. Actually, in the present results, one may think that gamma is almost constant in Fig. 12 except one point at the lowest Q. Therefore, to consider the Q dependency of the intensity (as seen in Fig. 11), the motion occurs in some confined space. If the fast component is attributed to an intermolecular motion as just discussed above, this intermediate component is more likely to be a rotation of water molecules. We need to further investigate this component.

V. DISCUSSION

As we have demonstrated above, by applying this analysis method to liquid water data, we have revealed the existence of an intermediate time-scale motion in water molecules. Moreover, by separating the intermediate-range mode from the spectrum, we could discuss two other motions more distinctly than has been done before. The model-free analysis allows us to reveal not only all diffusional aspects of new materials but also a new fact about molecular motion in a basic material such as water.

However, we must discuss here some MEM applications that require careful consideration. One of the points requiring care is the problem of peak separation in the results obtained from MEM analysis. For example, the MEM result sometimes shows only a single peak in the $B(Q = \text{const}, \Gamma)$ profile, although two isolated peaks exist at the same Q in the actual $B(Q,\Gamma)$. In Fig. 10, two peaks exist in the low-Q region (0.3–1.1 Å^{-1}) and they merge into a single peak at a higher Q. This merging into a single peak arises discontinuously at around 1.1–1.2 Å^{-1}, although it might also appear more smoothly in this system. These artificial phenomena are caused

by the MEM analysis for $B(Q = \text{const}, \Gamma)$ profiles that contain closely located peaks.

On the other hand, the MEM result sometimes shows multiple or isolated peaks in the Q region in the $B(Q = \text{const}, \Gamma)$ profile, although there is only a single peak in the Q region in the actual $B(Q = \text{const}, \Gamma)$ profile. In the case of a very wide or an asymmetric peak such as the KWW function, this phenomenon is common, as seen in Figs. 6(b)–6(d). Such actual phenomena are also caused by MEM analysis, although the origin is a substantial problem in "inverse transform" rather than that in the MEM analysis. MEM operates to counteract peak splitting by inverse transform. The appearance of such an artificial phenomenon depends on measurement conditions such as statistical precision and energy range. However, it is difficult to eliminate the phenomenon by improving a measurement condition. Therefore, to distinguish a reliable result from an artificial phenomenon such as this, it is desirable to judge whether the result is consistent after constructing a contour map (such as Fig. 10) from consecutive Q data measured under the same condition.

VI. CONCLUSION

The mode-distribution analysis method developed in this study does not require a model for each material, unlike conventional methods; therefore, in this sense, this method is completely model free. For materials that have several modes, their measurement data can be analyzed without making any assumption about the number of modes. In addition, we can access the distribution of relaxation time, which can be important for characterizing the relaxation. For these reasons, our analysis method is versatile and valuable to our understanding of relaxation phenomena in materials.

Because neutron spectrometers have evolved in recent years, QENS data over a wide Q-E space can be easily obtained nowadays. Our analysis method could possibly maximize the capability for exploring spectra in a wide Q-E space, and it gave intuitive results for molecular and atomic relaxations. QENS measurements on various other samples could benefit from the use of this method; therefore, we plan to continue to apply our method to other QENS studies. We will also try to expand the time scale of the result by simultaneous analysis of data from a few spectrometers and are considering a comparison with simulated data. We are convinced that the analysis method shown here will become one of the standards of QENS data analysis.

ACKNOWLEDGMENTS

We would like to thank all members of the Neutron Science Section at MLF, J-PARC, for supporting our study. We express thanks to Professor M. Matsumoto, Dr. T. Yamada, and Dr. M. Nakada for their valuable discussions. The quasielastic neutron experiments on liquid water were performed in the MLF at J-PARC with the approval of J-PARC (Proposal No. 2009A0092).

[1] M. Bée, *Quasielastic Neutron Scattering: Principles and Applications in Solid State Chemistry, Biology and Material Science* (Adam Hilger, Bristol, 1988).
[2] R. N. Silver, D. S. Sivia, and J. E. Gubernatis, Phys. Rev. B **41**, 2380 (1990).
[3] J. E. Gubernatis, M. Jarrell, R. N. Silver, and D. S. Sivia, Phys. Rev. B **44**, 6011 (1991).
[4] S. W. Provencher, Makromol. Chem. **180**, 201 (1979); Comput. Phys. Commun. **27**, 213 (1982); **27**, 229 (1982).
[5] M. Sakata and M. Sato, Acta Crystallogr., Sect. A: Found. Crystallogr. **46**, 263 (1990).
[6] M. Takata, E. Nishibori, and M. Sakata, Z. Kristallogr. **71**, 216 (2001).
[7] C. P. Lindsey and G. D. Patterson, J. Chem. Phys. **73**, 3348 (1980).
[8] M. N. Berberan-Santos, E. N. Bodunov, and B. Valeur, Chem. Phys. **315**, 171 (2005), and references therein.
[9] P. von Blanckenhagen, Ber. Bunsenges. Phys. Chem. **76**, 891 (1972), and references therein.
[10] V. F. Sears, Can. J. Phys. **44**, 1299 (1966).
[11] J. Teixeira, M.-C. Bellissent-Funel, S. H. Chen, and A. J. Dianoux, Phys. Rev. A **31**, 1913 (1985).
[12] A. Faraone, L. Liu, and S.-H. Chen, J. Chem. Phys. **119**, 6302 (2003).
[13] S.-H. Chen, P. Gallo, F. Sciortino, and P. Tartaglia, Phys. Rev. E **56**, 4231 (1997).
[14] A. Cunsolo, A. Orecchini, C. Petrillo, and F. Sacchetti, J. Chem. Phys. **124**, 084503 (2006).
[15] J. Qvist, H. Schober, and B. Halle, J. Chem. Phys. **134**, 144508 (2011).
[16] K. Nakajima *et al.*, J. Phys. Soc. Jpn. **80** Suppl. B, SB028 (2011).
[17] M. Russina and F. Mezei, Nucl. Instrum. Methods Phys. Res., Sect. A **604**, 624 (2009).
[18] M. Nakamura, R. Kajimoto, Y. Inamura, F. Mizuno, M. Fujita, T.Yokoo, and M. Arai, J. Phys. Soc. Jpn. **78**, 093002 (2009).
[19] A. Zeidler, P. S. Salmon, H. E. Fischer, J. C. Neuefeind, J. M. Simonson, and T. E. Markland, J. Phys.: Condens. Matter **24**, 284126 (2012).